Stem Cell Reports
Article

ISSCR

OPEN ACCESS

Developmental thyroid disruption permanently affects the neuroglial output in the murine subventricular zone

Pieter Vancamp,[1] Karine Le Blay,[1] Lucile Butruille,[1] Anthony Sébillot,[1] Anita Boelen,[2] Barbara A. Demeneix,[1] and Sylvie Remaud[1,*]

[1]Laboratory Molecular Physiology and Adaptation, CNRS UMR 7221, Department Adaptations of Life, Muséum National d'Histoire Naturelle, 7 Rue Cuvier, 75005 Paris, France

[2]Endocrine Laboratory, Department of Clinical Chemistry, Amsterdam UMC, University of Amsterdam, 1105 Amsterdam, the Netherlands

*Correspondence: sremaud@mnhn.fr

https://doi.org/10.1016/j.stemcr.2022.01.002

SUMMARY

Neural stem cells (NSCs) in the adult brain are a source of neural cells for brain injury repair. We investigated whether their capacity to generate new neurons and glia is determined by thyroid hormone (TH) during development because serum levels peak during postnatal reorganization of the main NSC niche, the subventricular zone (SVZ). Re-analysis of mouse transcriptome data revealed increased expression of TH transporters and deiodinases in postnatal SVZ NSCs, promoting local TH action, concomitant with a burst in neurogenesis. Inducing developmental hypothyroidism reduced NSC proliferation, disrupted expression of genes implicated in NSC determination and TH signaling, and altered the neuron/glia output in newborns. Three-month-old adult mice recovering from developmental hypothyroidism had fewer olfactory interneurons and underperformed on short-memory odor tests, dependent on SVZ neurogenesis. Our data provide readouts permitting comparison with adverse long-term events following thyroid disruptor exposure and ideas regarding the etiology of prevalent neurodegenerative diseases in industrialized countries.

INTRODUCTION

Distinct regions in the adult mammalian brain harbor neural stem cells (NSCs) that proliferate well beyond development and sustain life-long generation of new neural cells. The largest area is the subventricular zone (SVZ) lining the lateral forebrain ventricles. Under physiological conditions in mice, SVZ NSCs are primarily a source of neuroblasts and, less commonly, oligodendrocyte precursor cells (OPCs) (Menn et al., 2006). Neuroblasts migrate along the rostral migratory stream to integrate olfactory bulb networks, ensuring olfactory function (Lim and Alvarez-Buylla, 2016). OPCs populate nearby tissues, notably the *corpus callosum*, and differentiate into myelinating oligodendrocytes (Menn et al., 2006).

SVZ NSCs originate from radial glia of the embryonic ventricular zone (VZ)-SVZ (Fuentealba et al., 2015; Merkle et al., 2004). A single-cell RNA sequencing (RNA-seq) analysis on mouse SVZ cells isolated throughout development revealed that embryonically produced NSCs reactivate and acquire their definitive neurogliogenic identity between postnatal day 7 (P7) and P20 (Borrett et al., 2020), establishing a stable neuron/glia output thereafter. However, the factors governing this transition remain elusive. We hypothesized that thyroid hormone (TH) could fulfill this role because this endocrine cue also coordinates development of other brain regions (Williams, 2008). A postnatal TH peak conserved across the vertebrate lineage coincides with the transition from a plastic, developmental state to a mature brain in terms of cytoarchitecture and function (Gothié et al., 2020; Hadj-Sahraoui et al., 2000). Exposing rodents to hypothyroidism-inducing goitrogens dysregulates processes underlying corticogenesis, which, depending on the timing of exposure, include NSC proliferation, fate choice, migration, and differentiation (Moog et al., 2017). In the subgranular zone of the hippocampal dentate gyrus, another important NSC zone where life-long neurogenesis modulates learning- and memory-dependent plasticity, hypothyroidism in rats from P10–P21 reduced cell proliferation and stalled neurogenesis up until P90, the latest investigated time point (Zhang et al., 2009). Structural alterations can be irreversible, depending on the duration and the intensity of a hypothyroid insult, and negatively affect associated cognitive and motor skills in adult animals (Amano et al., 2018; Gilbert et al., 2017).

The biologically most active TH, 3,5,3′-triiodothyronine (T_3), modulates gene transcriptional activity through TH receptor α (TRα) to modulate NSC renewal and promote neuronal commitment in the adult mouse SVZ (Gothié et al., 2017; Lemkine et al., 2005; López-Juárez et al., 2012; Remaud et al., 2017). Increased intracellular T_3 in amplifying neuroprogenitors relieved arrested *Sox2* expression, favoring neuronal commitment (López-Juárez et al., 2012), whereas reduced T_3 action downregulated *Egfr*, favoring OPC fate (Remaud et al., 2017). Correspondingly, adult-onset hypothyroidism reduced neuroblast output and increased SVZ-derived OPC generation (Gothié et al., 2017). These observations in the adult mouse raise the question of whether local TH signaling acts similarly to determine later-life NSC properties during postnatal SVZ

development. Regulators of TH availability confine T_3 action in a brain-cell type-specific manner. These include the main TH transporters OATP1C1, taking up T_4, and MCT8, taking up T_3 and T_4 (López-Espíndola et al., 2019; Roberts et al., 2008; Wilpert et al., 2020); deiodinase type 2 (DIO2), activating T_4 into T_3; and DIO3, inactivating T_3 and T_4 (Bárez-López and Guadaño-Ferraz, 2017; Bianco et al., 2019). Discerning their expression patterns in the developing SVZ allows identification of TH target cell populations and, hence, those potentially vulnerable to TH signaling disruption.

These questions are central in stem cell biology because SVZ NSCs are an endogenous source of new neurons and glia that could facilitate CNS injury repair (Vancamp et al., 2020a). Additionally, mounting evidence shows that developmental exposure to endocrine-disrupting chemicals (EDCs) that alter TH homeostasis (Boas et al., 2012) evoke adverse and sometimes irreversible effects on the fetal/postnatal brain (Mughal et al., 2018) but with a so far unknown effect on (SVZ-)NSCs. Epidemiological data already showed that slight variations in TH levels during fetal development not only reduce human offspring IQ but also impair lineage decisions, as reflected by altered gray/white matter ratios (Korevaar et al., 2016).

Here we investigated TH regulator expression during postnatal SVZ remodeling by re-analyzing publicly available single-cell RNA-seq data and using RNAscope. Then we determined how ablating the postnatal TH peak by 6-n-propyl-2-thiouracil (PTU)-induced hypothyroidism affects the murine SVZ in the short and long term, in particular neuron/glia output and olfactory behavior. We identified the developing SVZ as a tissue sensitive to aberrant TH signaling, pinpointing various processes of interest when studying the effect of EDCs.

RESULTS

TH regulators are dynamically expressed in the postnatal SVZ

To grasp how TH availability is regulated in different SVZ cell types before and after the TH peak, we re-analyzed single-cell RNA-seq data obtained from P2 and P20 SVZ cells of *Emx1-Cre;R26-LSL-EYFP* mice (Borrett et al., 2020) using the Seurat v.3.0 toolkit (Stuart et al., 2019). Following integration and two-dimensional reduction, we plotted SVZ cell-type-specific markers (Zywitza et al., 2018) and isolated 12 cell clusters (Figure S1). Five were of interest for our study, recapitulating neuronal versus glial lineages: NSCs, transient amplifying progenitors (TAPs), glia (astrocytes and OPCs), and neuroblasts (Figure 1A). Astrocyte and NSC proportions at P20 were higher than at P2, at the expense of TAPs and neuroblasts. OPC numbers remained stable (Figure 1A).

We then examined expression of TH regulators and neuroglial cell markers within these isolated cell populations. *Dio2* was mainly enriched in a subpopulation of astrocytes and in some NSCs at P20. Some NSCs also expressed *Dio3* (Figures 1B and 1C). *Thra*, encoding TRα1 and TRα2, was ubiquitously expressed in SVZ cells at P2 and P20, whereas *Thrb* was expressed in only a few cells across the different categories (Figures 1B and S2), as expected (Lemkine et al., 2005). Compared with P2, many NSCs increasingly expressed *Oatp1c1* and, to a minor extent, *Mct8* at P20. Astrocytes predominantly expressed *Oatp1c1* at P20 (Figures 1B and 1C). Yellow colors on the cluster plots show *Mct8* and *Oatp1c1* overlapping in an important fraction of SVZ NSCs and astrocytes at P20 (Figures 1C and S2). Almost none of the *Dio3*+ cells co-expressed neither of the TH transporters (Figure S3). Several neuroblasts also expressed *Mct8*, but only at P2 (Figures 1B and 1C). At P20, both transporters were also enriched in epithelial and endothelial cells forming the blood-cerebrospinal fluid and blood-brain barrier (BBB), respectively (Figure S4). Absence of endothelial cell expression at P2 suggests that TH uptake in the SVZ occurs predominantly via BBB-independent routes before the TH peak.

Expression of the positively regulated T_3 target gene *Krüppel-like factor 9* (*Klf9*) (Dugas et al., 2012) was higher at P20, whereas the negatively regulated *Musashi-1* (*Msi1*) (López-Juárez et al., 2012) displayed an inverse pattern (Figures 1D and S2). Among the neuroglia markers, *Olig2* was enriched in P2 astrocytes and in OPCs in which a concomitant rise in *Ng2* corresponded to a postnatal wave of oligodendrogenesis (Vancamp et al., 2020b; Figure 1D). As expected, *Dlx2* and *Doublecortin* (*Dcx*) marked early committed neuroprogenitors and neuroblasts, respectively. A few *Dlx2*+ NSCs indicated neuronal lineage commitment while their transcriptional profile still assigned a stem cell identity.

To validate the findings from our *in silico* analysis, we combined RNAscope, visualizing single mRNA transcripts, to SOX2 immunohistochemistry (IHC), a marker of progenitor pluripotency, on coronal SVZ sections at P4 and P21 (Figures 1E and 1F). Average *Thra*, *Klf9*, and *Mct8* mRNA transcript numbers increased in the majority of SOX2+ cells (Figure 1F), as observed before (Figures 1B–1D), whereas cellular *Dio3* expression remained low from P4–P21. IHC showed that this coincided with elevated TRα1 levels in SOX2+ SVZ progenitors after the TH peak (Figure 1G).

Overall, the dynamically increased TH regulator expression in SVZ NSCs and astrocytes after the TH peak suggests that they are primary TH targets and possess all molecular machinery to promote TH action during postnatal SVZ reorganization.

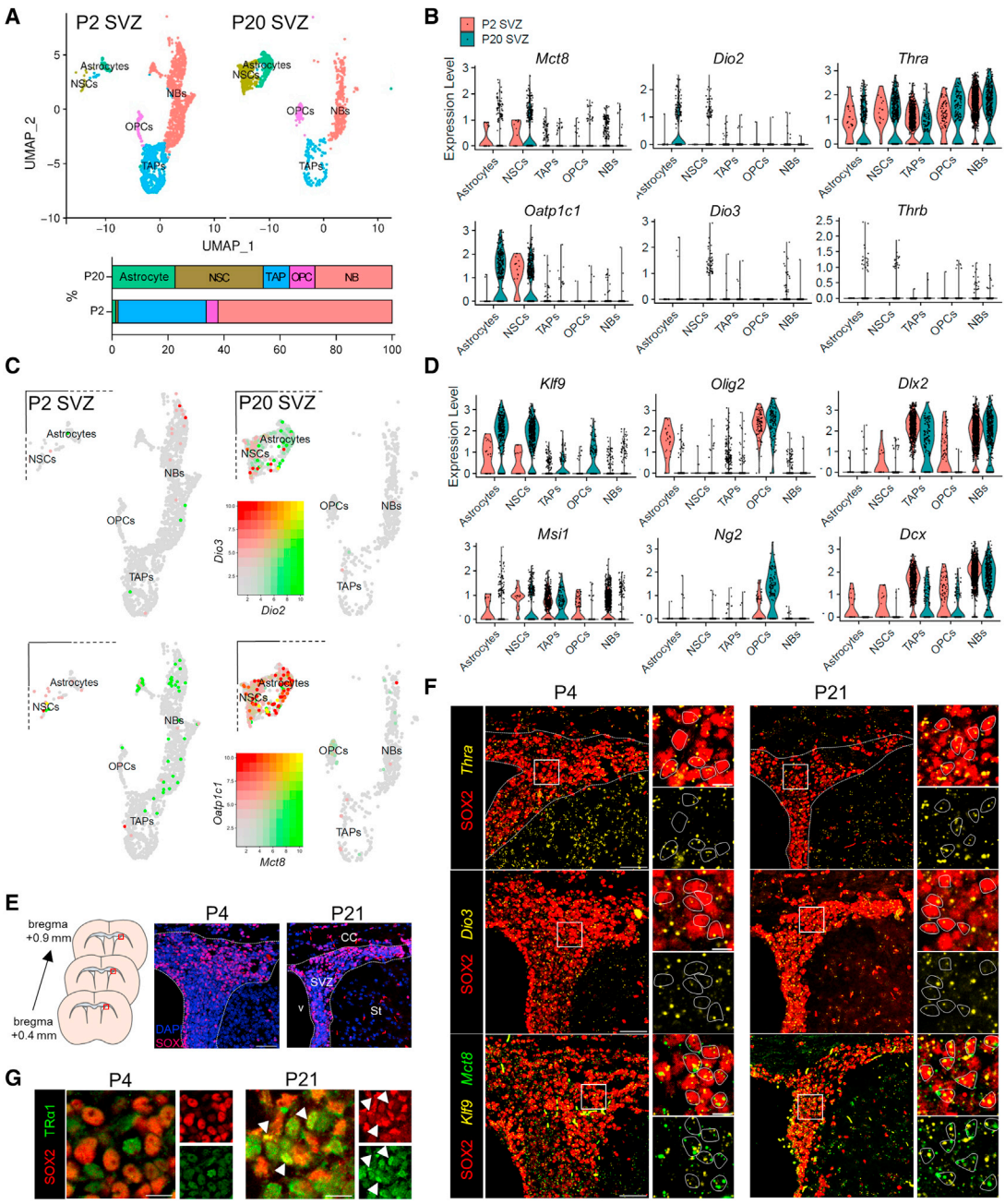

Figure 1. Cellular reorganization and dynamic expression of TH pathway and neuroglial genes in SVZ cell populations before and after the TH peak

(A) Two-dimensional UMAP plots showing five isolated SVZ cell clusters of interest at P2 and P20 after integrated single-cell RNA-seq re-analysis (see also Figure S1). The bottom panel shows the proportion of each cell type relative to total cell numbers in the five clusters.

(B) Violin plots showing expression of the TH transporters *Mct8* and *Oatp1c1*, the deiodinases *Dio2* and *Dio3*, and the two TR-encoding genes *Thra* and *Thrb* in the SVZ cell clusters at P2 (red) and P20 (dark green) (see also Figure S2).

(C) Cluster plots mapping cell-specific expression patterns of *Mct8*, *Oatp1c1*, *Dio2*, and *Dio3* (see also Figures S3 and S4).

(D) Violin plots showing expression of the positively and negatively TH-regulated genes *Klf9* and *Msi1*, respectively; the pro-oligodendrogenic genes *Olig2* and *Ng2*; and the pro-neuronal genes *Dlx2* and *Dcx*.

(E) Schematic overview and pictures of the P4 and P21 SVZ (area within white dotted lines).

(F) Representative RNAscope pictures showing expression of TH-regulated genes in SOX2+ SVZ progenitors (white circles). Scale bars, 50 μm and 10 μm (inserts).

(legend continued on next page)

Developmental hypothyroidism alters TH regulator and neuroglial gene expression in the postnatal SVZ

To study how ablation of the TH peak affects cellular TH signaling and neuroglial commitment, we fed pregnant dams a 0.15% PTU-enriched diet that blocks TH synthesis, exposing the progeny from embryonic day 15 (E15)–P21. Newborns weighed less at P15–P21 (Šidák test following two-way ANOVA, $F_{1,48} = 115.7$, $p < 0.0001$) (Figure 2A). Serum T_4 and T_3 levels in PTU-treated P4 and P15 mice were lower than the mass spectrometry detection threshold (<0.2 and <0.1 nmol/L, respectively), whereas concentrations peaked in P15 control animals (Figure 2B).

We then examined expression of genes associated with TH signaling and neuroglial commitment in dissected SVZs from P4–P21. A heatmap depicts the relative changes in gene expression compared with P4 controls for each gene (Figure 2C; see fold changes in Table S1). Under normal conditions, rising *Dio2*, *Oatp1c1*, and *Klf9* over the course of postnatal development indicated increased TH action.

When comparing numbers of the 13 tested genes between controls and PTU-treated SVZs, 2 were up- and 7 were downregulated at some point, with a maximum of 6 differentially expressed genes at P15. Only at P4 were no genes affected. Increased *Dio2* (two-way ANOVA, $F_{1,30} = 19.32$, $p = 0.0001$) together with decreased *Dio3* expression ($F_{1,30} = 28.11$, $p < 0.0001$) is a classic sign of hypothyroidism (Hernandez et al., 2012), and we observed these indications of low TH levels in SVZ tissue from P8 onward (Figure 2C).

At P15, 4 key neurogliogenic genes were downregulated: the multipotent NSC/progenitor marker *Sox2* (Šidák test following two-way ANOVA, $t_{30} = 3.705$, $p = 0.0034$), *Dlx2* ($t_{30} = 3.464$, $p = 0.0065$), *Dcx* ($t_{30} = 2.977$, $p = 0.0226$), and the oligodendroglial cell marker *Olig2* ($t_{30} = 4.116$, $p = 0.0011$). The latter was still downregulated at P21 ($t_{30} = 3.639$, $p = 0.0041$), whereas it gradually increased under control conditions (Figure 2C). By combining RNAscope with IHC at P21 and counting single mRNA transcripts in randomly selected SOX2+ cells, we confirmed upregulated *Dio2* (t test, $t_5 = 4.377$, $p = 0.0072$), and downregulated *Dio3* (Mann-Whitney *U* test, $p = 0.029$) and *Klf9* (t test, $t_6 = 3.427$, $p = 0.014$) in SVZ progenitors of PTU-exposed mice (Figure 2D).

These results indicate that developmental hypothyroidism alters transcription patterns of TH-responsive genes and those involved in NSC/TAP maintenance and commitment.

Developmental hypothyroidism alters neurogliogenesis in the postnatal SVZ

We then studied SVZ neuroblast and OPC generation before (P4) and after the TH peak (P21) using antibodies against DCX and OLIG2, respectively (Figure 3A). We distinguished between the dorsal and lateroventral (LV) SVZ because recent data demonstrated that these microdomains have different neuroglia outputs (e.g., Mizrak et al., 2019). Under both conditions, almost exclusively OLIG2+ OPCs were generated at P4, whereas a burst in DCX+ neuroblasts was observed at P21 in both microdomains (Figure 3B). The OPC density in the dorsal SVZ was similar as a function of age (two-way ANOVA, $F_{1,21} = 1.678$, $p = 0.21$) and not affected by hypothyroidism ($F_{1,21} = 0.011$, $p = 0.92$). In contrast, the density of DCX+ neuroblasts was 40% lower in P21 PTU-treated animals (Tukey test following two-way ANOVA, $q_{21} = 8.36$, $p < 0.0001$).

The LV SVZ was thinner under hypothyroid conditions (Tukey test following two-way ANOVA; P4: $q_{17} = 4.921$, $p = 0.014$; P21: $q_{17} = 4.154$, $p = 0.041$) (Figure 3C). At P21, OLIG2+ cell numbers in PTU-treated animals were only one-10th that of controls (Tukey test following two-way ANOVA, $q_{21} = 6.67$, $p = 0.0006$). DCX+ neuroblast numbers increased from P4 to P21 and were reduced by PTU at P21 ($q_{21} = 4.05$, $p = 0.043$) (Figure 3D). Hence, developmental hypothyroidism reduces postnatal neurogenesis in the P21 SVZ and oligodendrogenesis in the LV SVZ.

Last, we calculated the proportion of DCX+ versus OLIG2+ cells, reflecting the neuron/glia balance (Figure 3E). As observed with IHC, the dorsal SVZ output was predominantly gliogenic at P4. At P21, however, more than 80% of committed cells were DCX+. The neuron/glia ratio in the dorsal SVZ did not change under hypothyroid conditions (two-way ANOVA, $F_{1,21} = 0.769$, $p = 0.39$). In the LV SVZ, the neuron/glia ratio changed from 62/28% to 90/10% at P21 following PTU exposure (Tukey test following two-way ANOVA, $q_{21} = 8.10$, $p < 0.0001$) (Figure 3E).

Developmental hypothyroidism reduces postnatal SVZ NSC proliferation and increases the progenitor pool

Next we assessed progenitor behavior using antibodies against SOX2 to label NSC/progenitors and PH3 for mitotic cells (Figure 4A). In the dorsal SVZ, SOX2+ cell densities were more than 2- and 3-fold higher, respectively, under PTU conditions at P4 (Tukey test following two-way ANOVA, $q_{19} = 4.88$, $p = 0.013$) and P21 ($q_{19} = 9.08$, $p < 0.0001$) compared with controls (Figures 4A and 4B). Densities of PH3+ cells were reduced 2-fold under hypothyroid

(G) Pictures showing TRα1 in SOX2+ SVZ progenitors at P21. White arrows mark co-expression. Scale bar, 10 μm. CC, *corpus callosum*; NB, neuroblast; NSC, neural stem cell; OPC, oligodendrocyte precursor cell; St, striatum; SVZ, subventricular zone; TAP, transient amplifying progenitor; v, ventricle. See also Figures S1–S4.

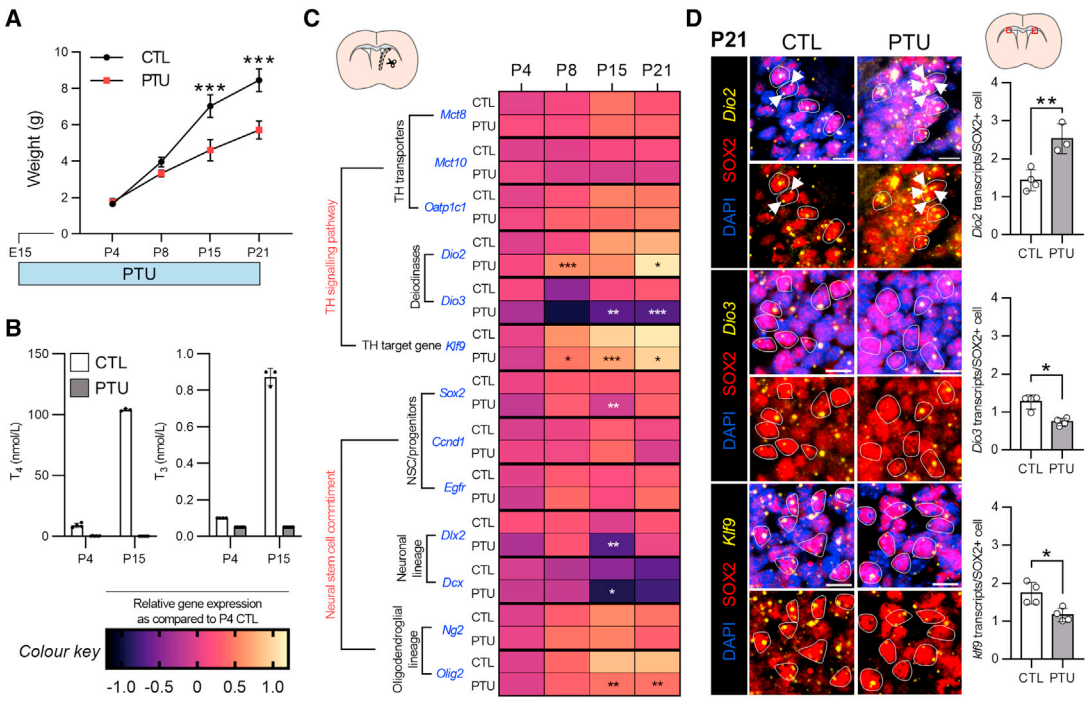

Figure 2. Developmental PTU treatment alters expression of TH regulator genes and markers for neuroglial commitment

(A) Graph (mean ± SD) showing slower weight gain in hypothyroid newborn mice at P15–P21.

(B) Graphs (mean ± SD) showing serum T_4 and T_3 levels (nmol/L) at P4 and P15 in control (CTL) and PTU-treated mice (n = 3–6).

(C) Heatmap showing relative changes (log-transformed data) in expression of genes (blue) within the TH signaling pathway and those implicated in NSC commitment compared with control animals at P4 for each gene (set to 0). n = 4–6 replicates/group (SVZs of 3 mice/replicate), two-way ANOVA followed by Šidák post hoc test (see Figure S2 for fold changes).

(D) Representative RNAscope pictures showing TH target gene expression in SOX2+ SVZ progenitors (white circles) in CTL and PTU animals at P21. Each yellow dot represents one mRNA transcript (white arrows) (n = 3–4/group; *Dio2* and *Klf9*, two-tailed t-tests; *Dio3*, Mann-Whitney *U* test). Graphs show mean ± SD. Scale bars, 10 μm.

*p < 0.05; **p < 0.01; ***p < 0.001. See also Table S1.

conditions at P21 (Tukey test following two-way ANOVA, $q_{19} = 5.05$, $p = 0.011$) but not at P4 ($q_{19} = 1.86$, $p = 0.57$) (Figure 4B).

In the LV SVZ, SOX2+ cell numbers were 2-fold higher following PTU exposure at P4 only (Tukey test following two-way ANOVA, $q_{19} = 6.60$, $p = 0.0009$). PH3+ cell numbers were lower at P4 (Tukey test following two-way ANOVA, $q_{19} = 6.10$, $p = 0.0019$) and P21 in PTU conditions versus controls ($q_{19} = 4.80$, $p = 0.015$) (Figures 4C and 4D). These data show that postnatal SVZ progenitors proliferate less under hypothyroid conditions, whereas a larger progenitor pool suggests a blocked cell cycle, as observed before (Lemkine et al., 2005).

In vitro neurospheres prepared from PTU-treated P21 newborns are less responsive to T_3

Next we prepared *in vitro* neurospheres from dissected SVZs of control and PTU-treated mice and allowed them to proliferate for 7 days, and then differentiate for 7 days with or without 1 or 50 nM exogenous T_3 (Figure 5A).

At P4, around 5% of the SVZ progenitors dissected from control or PTU-treated mice were OLIG2+, and 40% were DCX+, a ratio that did not change under added T_3 (Figures 5B and 5C). However, at P21, T_3 treatment increased the proportions of OLIG2+ OPCs in neurospheres derived from control animals (10% versus 5%, Tukey test following two-way ANOVA, $q_{161} = 6.159$, $p = 0.0003$) but not in those dissected from PTU-treated animals ($q_{161} = 3.255$, $p = 0.199$) (Figures 5D and 5E). Similarly, the proportion of DCX+ cells decreased after T_3 treatment, but only in neurospheres prepared from control animals (18% versus 33%, $q_{161} = 6.887$, $p < 0.0001$). Consequently, DCX+ proportions were lower under 50 nM T_3 treatment in neurospheres prepared from PTU-treated animals compared to those prepared from control animals ($q_{161} = 4.366$, $p = 0.0282$).

As a result, in neurospheres prepared from control P21 mice, the neuron/glia balance decreased by 22% following addition of 50 nM T_3 (Tukey test following two-way ANOVA, $q_{161} = 8.752$, $p < 0.0001$) but did not change in

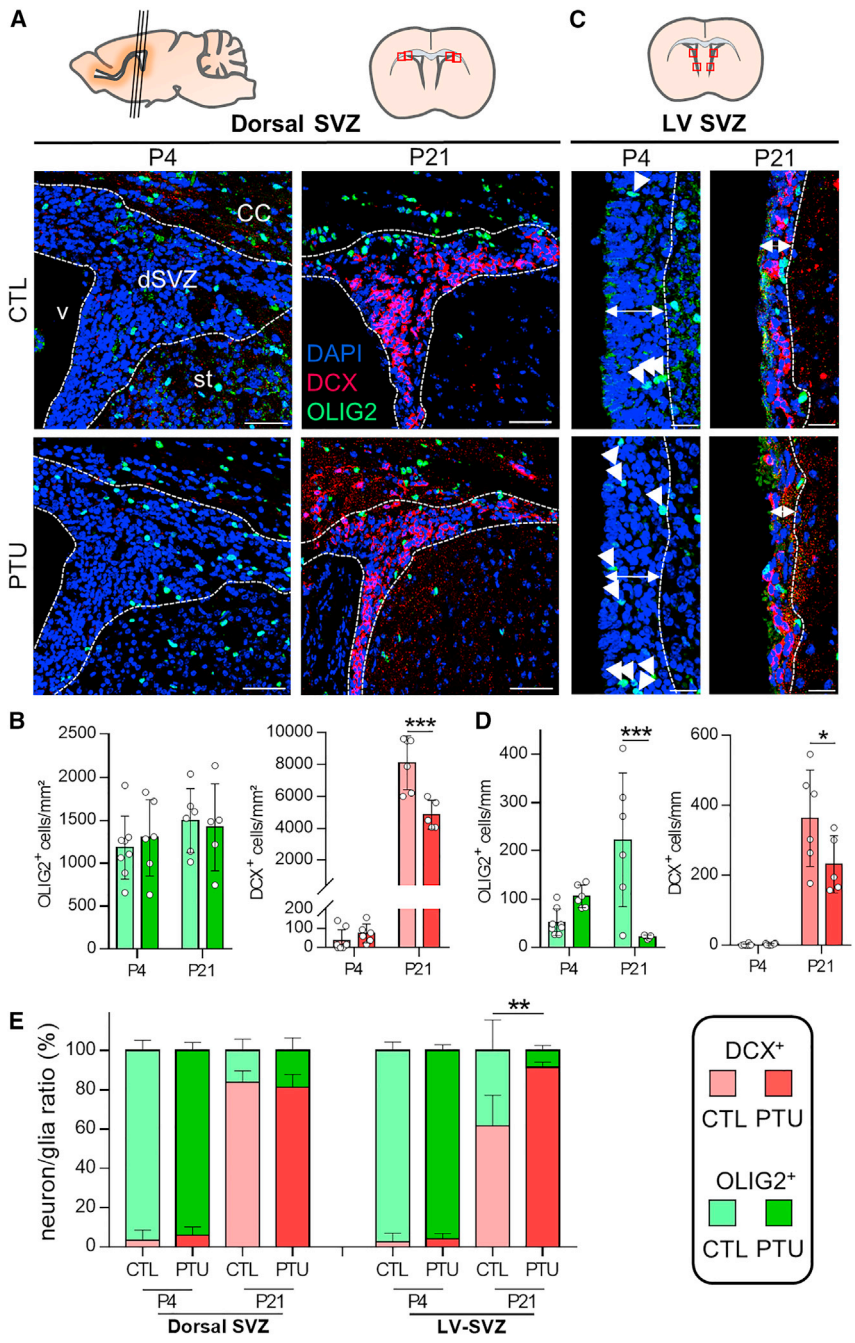

Figure 3. Developmental PTU treatment affects SVZ neurogliogenesis at P21

(A) Representative IHC pictures of DCX+ neuroblasts (red) and OLIG2+ OPCs (green) on coronal sections of the dorsal SVZ. At P4, almost exclusively OLIG2+ OPCs are observed (left panels). Counts were performed in the area delineated by the red boxes on 3–4 sections/animal. A burst of DCX+ neuroblasts was observed at P21 (right panels). Scale bars, 50 μm.

(B) Graphs (mean ± SD) showing densities of OLIG2+ and DCX+ cells in the dorsal SVZ (area within white dotted lines in A).

(C) Representative IHC pictures of DCX+ neuroblasts and OLIG2+ OPCs on coronal sections of the LV SVZ. Scale bars, 20 μm.

(D) Graphs (mean ± SD) showing the numbers of OLIG2+ cells and DCX+ cells (per mm) in the LV SVZ.

(E) The neuron/glia balance was calculated as the ratio between DCX+/DCX+ OLIG2+ cells versus OLIG2+/DCX+ OLIG2+ cells. Plots depict mean ± SD. n = 5–8/group, two-way ANOVAs followed by Tukey post hoc tests. dSVZ, dorsal SVZ; LV, lateroventral. *p < 0.05; ***p < 0.001.

cells cultured from PTU-treated mice (q_{161} = 3.571, p = 0.123) (Figure 5F). In other words, the neuron/glia ratio in 50 nM T_3-treated cell cultures derived from control P21 mice changed from 83%/17% to 61%/39% while remaining at ±80%/20% in cultures of PTU-treated P21 mice. These results suggest that SVZ NSC/progenitors are particularly sensitive to T_3 after the TH peak, echoing our *in vivo* data. They lose their responsiveness to T_3 following developmental hypothyroidism.

Transient developmental hypothyroidism persistently impairs SVZ neurogliogenesis and behavior in adult mice

Last, we examined P100 mice that were fed a normal diet after PTU exposure from E15–P21. Adult mice developmentally treated with PTU did not reach a normal weight (t test, t_8 = 3.158, p = 0.0134) (Figure 6A). Mass spectrometry analysis revealed normalization of serum T_4 levels (t test, t_8 = 0.330, p = 0.75) but borderline significantly lower T_3 (t_8 =

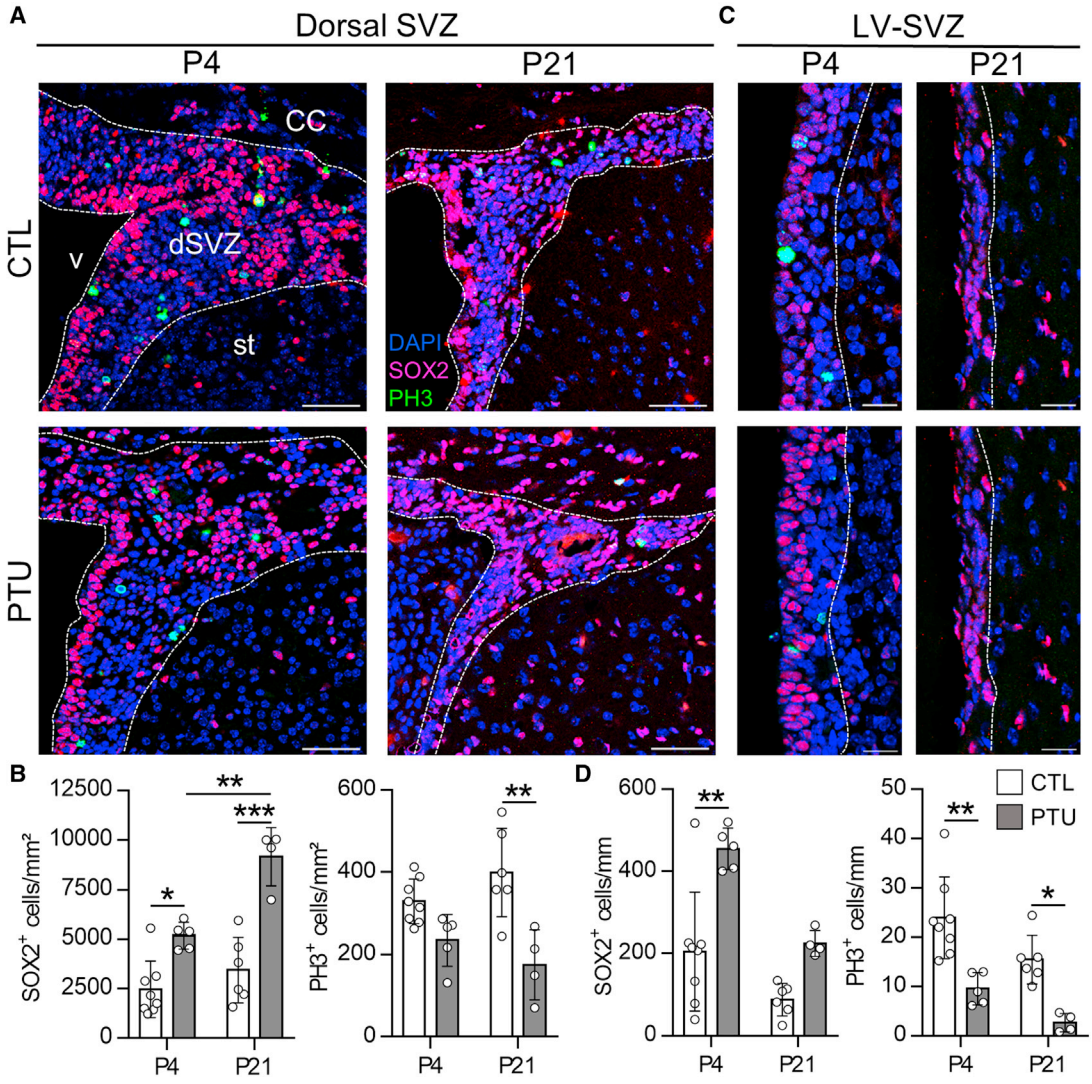

Figure 4. Developmental PTU treatment increases SOX2+ progenitors and reduces mitosis in the postnatal SVZ

(A) Representative IHC pictures of PH3+ mitotic cells (green) and SOX2+ progenitors (red) on coronal sections of the dSVZ. Scale bars, 50 μm.

(B) Graphs (mean ± SD) showing densities of PH3+ and SOX2+ cells in the dSVZ (area within white dotted lines in A).

(C) Representative IHC pictures of PH3+ mitotic cells and SOX2+ progenitors on coronal sections of the LV SVZ. Scale bars, 20 μm.

(D) Graphs (mean ± SD) showing numbers of PH3+ and SOX2+ cells (per mm) in the LV SVZ. Plots depict mean ± SD. n = 4–8/group, two-way ANOVAs followed by Tukey post hoc tests. *p < 0.05; **p < 0.01; ***p < 0.001.

2.141, p = 0.0647) and increased reverse T_3 (rT_3) levels (Mann-Whitney *U* test, p = 0.0159) (Figure 6A), suggesting persistent thyroid axis alterations.

A last set of experiments analyzed long-lasting consequences on NSC fate and associated behavior. Olfactory memory in mice relies on a supply of SVZ-derived neuroblasts (Lim and Alvarez-Buylla, 2016). Adult mice underwent an olfactory habituation-dishabituation test with five non-social and social odors (Figure 6B). The investigation time of an odor indicated their ability to habituate and dishabituate each time a new odor was presented. Developmentally PTU-treated mice spent less time investigating male urine as compared to controls (Bonferroni test following two-way ANOVA, $t_{60} = 8.328$, $p < 0.001$). Apart from that, all mice successfully discriminated other odors with equal success.

Then we measured the investigation time 2, 30, and 60 min after presenting an odor (almond) to assess short-term olfactory memory. In control mice, investigation time dropped with each presentation (habituation). In

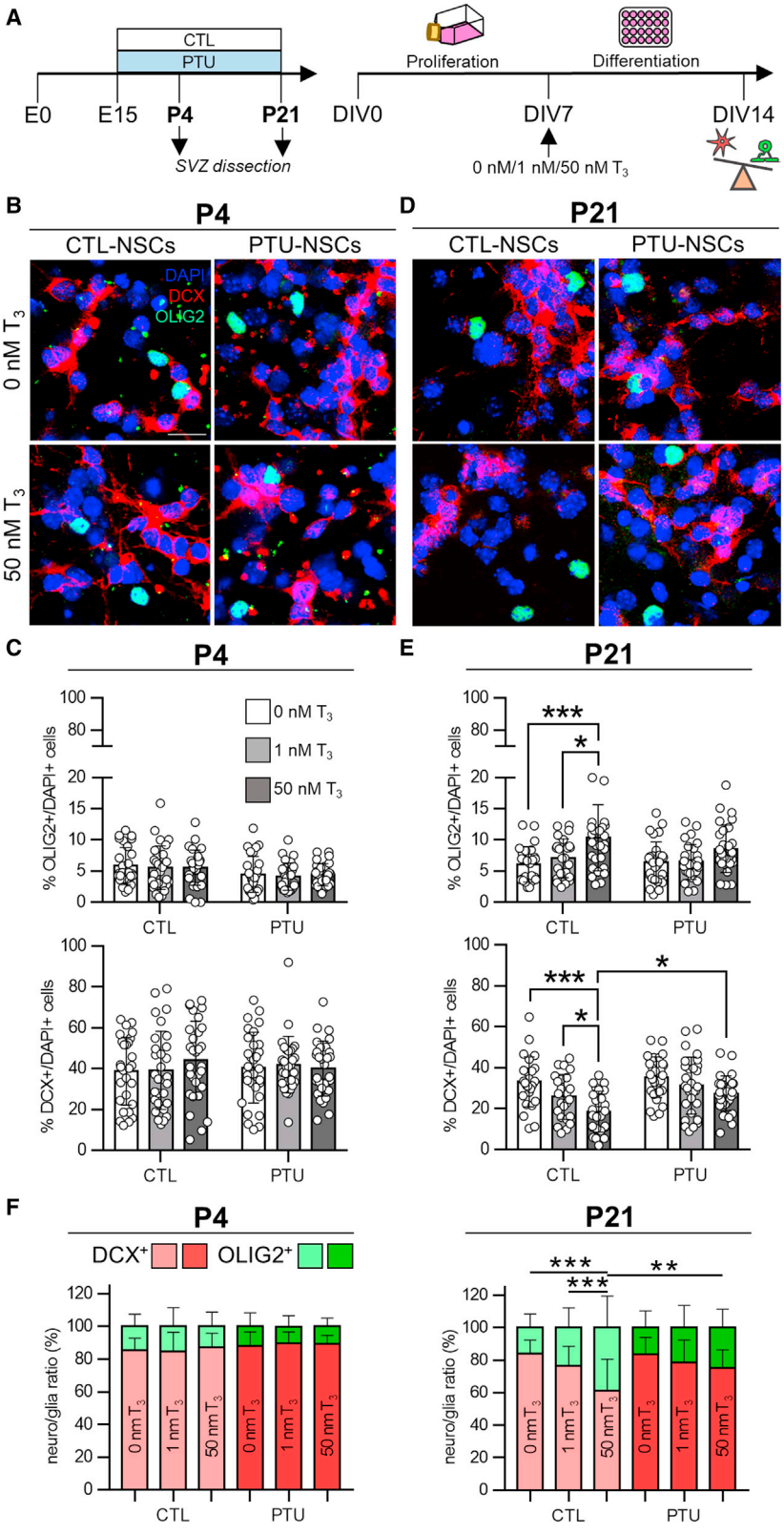

Figure 5. T_3 affects neither the neuron/glia balance nor differentiation in SVZ NSC/progenitors from PTU-treated mice

(A) Schematic overview of the neurosphere assay.

(B) Representative IHC pictures of DCX+ neuroblasts (red) and OLIG2+ OPCs (green) differentiated from SVZ NSC/progenitors isolated from CTL and PTU-treated P4 animals. Scale bar, 10 μm.

(C) Graphs (mean ± SD) showing the proportion of DCX+ and OLIG2+ cells in the DAPI+ cell population at P4.

(D) Representative pictures of DCX+ neuroblasts and OLIG2+ OPCs differentiated from SVZ NSC/progenitors isolated from CTL and PTU-treated P21 animals. Note the lower proportion of differentiated cells and fewer DCX+ neuroblasts in the bottom left panel (CTL, 50 nM T_3).

(E) Graphs (mean ± SD) showing the proportion of DCX+ and OLIG2+ cells in the DAPI+ cell population at P21.

(F) Graphs (mean ± SD) showing the ratio of DCX+ versus OLIG2+ cells, reflecting the neuron/glia balance. Plots depict mean ± SD (24–30 images/group; data are from 3 independent experiments). Two-way ANOVAs followed by Tukey post hoc tests. DIV, days *in vitro*. *p < 0.05; **p < 0.01; ***p < 0.001.

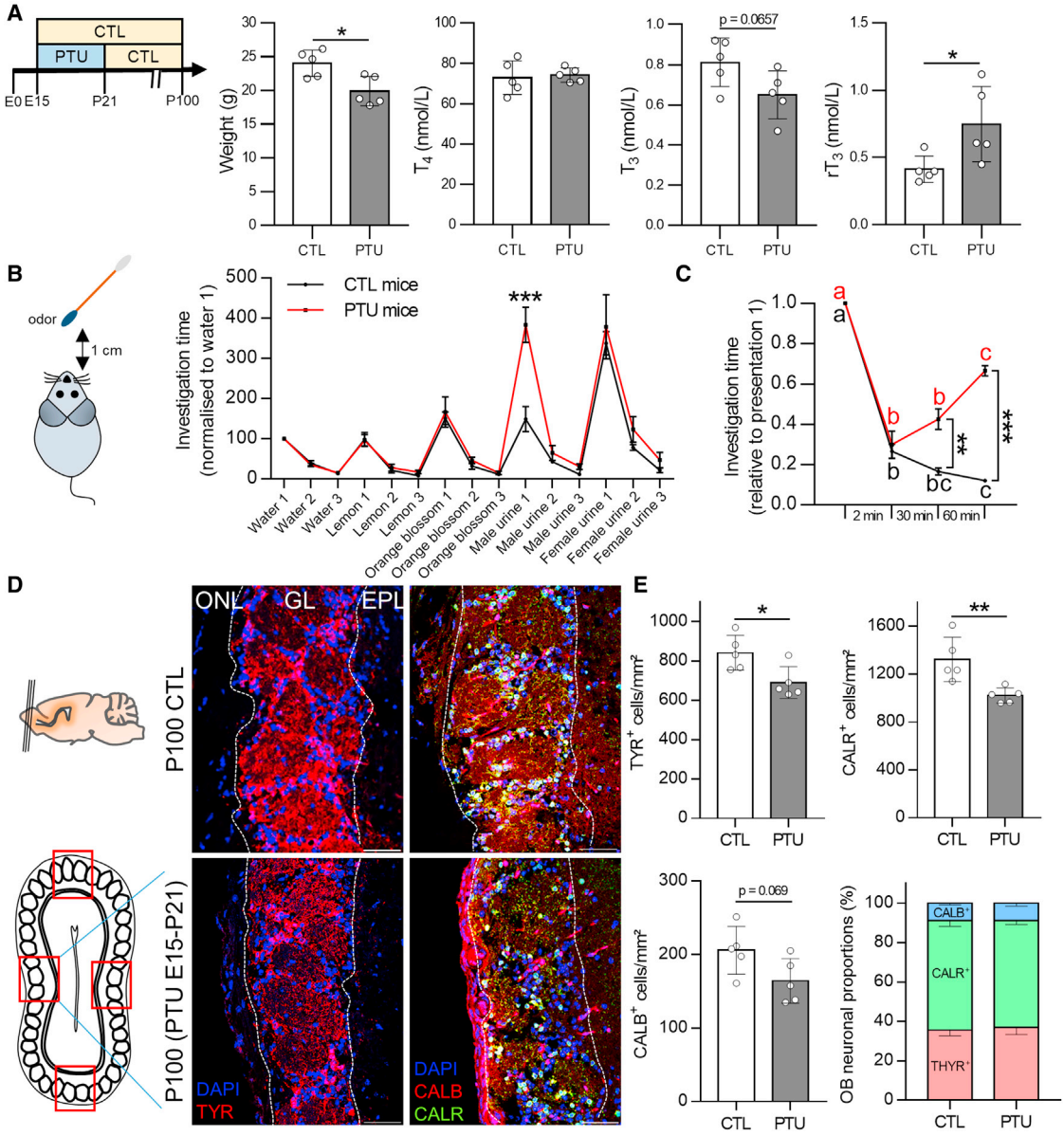

Figure 6. Impaired short-term olfactory memory and olfactory bulb cytoarchitecture in adult mice developmentally exposed to PTU

(A) Graphs (mean ± SD) showing weight and serum T_4, T_3, and rT_3 levels (nmol/L) in P100 control mice and those developmentally treated with PTU (n = 5/group).

(B) Graph (habituation-dishabituation test) showing investigation time following three consecutive presentations of odors relative to water 1.

(C) Graph (short-term odor memory test) showing the relative investigation time 2 (habituation), 30 and 60 min after presentation of the same odor (short-term memory). Graphs in B and C depict mean ± SEM (n = 5/group, Bonferroni post hoc tests following two-way ANOVAs). Asterisks mark differences between groups at one time point and letters between time points within one group.

(D) Representative IHC pictures in the glomerular layer (white dotted lines) of the olfactory bulbs (red box on schematic section) for tyrosine hydroxylase+ (red, left pictures), calretinin+ (green, right pictures), and calbindin+ neurons (red, right pictures). Scale bars, 50 μm.

(E) Graphs (mean ± SD) showing neuronal densities in the glomerular layer (n = 5/group, unpaired t tests). The bottom right graph shows the relative proportions of the neuronal subtypes. CALB, calbindin; CALR, calretinin; EPL, external plexiform layer; GL, glomerular layer; ONL, olfactory nerve layer; TYR, tyrosine hydroxylase.*p < 0.05; **p < 0.01; ***p < 0.001.

developmentally PTU-treated mice, investigation time increased again 30 min after the second and 60 min after the third presentation, differing significantly from control animals (Bonferroni test following two-way ANOVA; 30 min: $t_{16} = 4.321$, $p = 0.0021$; 60 min: $t_{16} = 9.056$, $p < 0.001$) (Figure 6C). This indicates that the ability to remember an odor over a short period is impaired in adult mice that were developmentally exposed to PTU.

To identify the cellular effects underlying this phenotype, we performed IHC for three types of interneurons in the olfactory bulb: calretinin, calbindin, and tyrosine hydroxylase (Figure 6D). The density of tyrosine hydroxylase+ neurons in the glomerular layer was decreased significantly (Mann-Whitney *U* test, $p = 0.0317$), as was that of calretinin+ neurons (t test, $t_8 = 3.434$, $p = 0.0089$), and borderline-significantly for calbindin+ neurons (t test, $t_8 = 2.098$, $p = 0.069$) (Figure 6E). Cell type proportions were unaltered.

We also assessed the cellular processes we examined previously (Figure 7A). The SVZ area was 20% smaller at P100 in mice developmentally exposed to PTU (data not shown; $t_8 = 2.463$, $p = 0.039$). DCX+ cell densities in the dorsal (t test, $t_8 = 0.4327$, $p = 0.68$) and LV SVZ (t test, $t_8 = 1.297$, $p = 0.23$) were similar in both groups (Figure 7B). However, because the SVZ was smaller, absolute neuroblast numbers were lower in developmentally PTU-exposed mice. OLIG2+ cell densities were almost 2-fold lower in the dorsal (t test, $t_8 = 2.926$, $p = 0.019$) and LV SVZ of adult mice developmentally exposed to PTU (t test, $t_8 = 3.112$, $p = 0.014$) (Figure 7B). This drop increased the neuron/glia balance in the dorsal SVZ from 86%/14% to 93%/7% (t test, $t_8 = 3.247$, $p = 0.012$), whereas it did not change in the LV SVZ (Figure 7C). These data indicate that SVZ neurogenesis in adult mice developmentally exposed to PTU recovers but that SVZ oligodendrogenesis remains impaired.

We also stained for SOX2 and PH3 as well as Ki67 to detect cycling cells (as in Vancamp et al., 2019; Figure 7D). SOX2+ cell numbers were 30% lower in the LV SVZ of developmentally PTU-exposed mice (t test, $t_8 = 2.901$, $p = 0.020$). The numbers of Ki67+ and PH3+ cells did not differ between conditions or SVZ microdomains (Figure 7E). The proliferation index, the proportion of PH3+ cells in the Ki67+ population, did not change, suggesting that the cell cycle was unaffected by developmental PTU exposure at this adult stage (Figure 7F).

DISCUSSION

The adult SVZ harbors the largest NSC population that generates new neuroblasts and OPCs throughout life in rodents. A single-cell RNA-seq analysis on mouse SVZ cells isolated throughout development estimated that NSCs, produced during embryonic development (Fuentealba et al., 2015), reactivate postnatally and acquire their future neurogliogenic identity between P7 and P20 (Borrett et al., 2020), establishing a stable neuron/glia output thereafter. The factors that govern this transition remain elusive. We hypothesized that TH could be one of them, given that serum TH levels rise postnatally and peak at P15 (Hadj-Sahraoui et al., 2000), TH orchestrates NSC processes underlying brain development (Moog et al., 2017), and TH controls NSC proliferation and fate choice in the adult mouse SVZ (Lemkine et al., 2005; López-Juárez et al., 2012).

First we re-explored the single-cell RNA-seq data generated from *Emx1-Cre;R26-LSL-EYFP* mice (Borrett et al., 2020). Compared with P2, SVZ NSC and astrocyte population sizes were 10 times larger at P20, whereas TAP numbers had decreased, reflecting the characteristic adult SVZ composition with few cycling progenitors. High *Dio2* levels in P20 astrocytes suggested increased conversion of T_4 into T_3, facilitating T_3 supply to SVZ NSCs enriched with *Mct8* and *Oatp1c1* (Luongo et al., 2021). At P20, brain-barrier cells were detectable, too, and expressed *Mct8* and *Oatp1c1*, as shown before (Roberts et al., 2008; Wilpert et al., 2020), indicating that TH uptake from the blood and cerebrospinal fluid to SVZ cells is put in place during the first postnatal weeks.

Our IHC data showed that this postnatal transition occurs simultaneously with a burst in neuroblasts, generating a stable neuron/glia output of 80%/20%, characteristic of adult mice and rats (Remaud et al., 2017; Zhang et al., 2009). The discrepancy between decreasing *Dcx* transcripts and more DCX+ neuroblasts from P4–P21 (compare Figures 2C and 3A), might reflect post-transcriptional mRNA repression in perinatal NSCs until molecular cues trigger translation into proteins. Similarly, some adult mouse SVZ cells expressed *Ttr*, whereas the encoding protein was undetectable (Vancamp et al., 2019). Sequencing individual mRNAs showed that NSC differentiation into neurons coincides with a dynamically changed translation of specific mRNAs and repression of *Sox2* (Baser et al., 2019), a key TH-responsive gatekeeper of NSC identity (López-Juárez et al., 2012). Such mechanisms bolster the hypothesis that the embryonically generated NSC pool (Fuentealba et al., 2015) reactivates postnatally to establish neuroglial identities (Rushing and Ihrie, 2016), with TH potentially exerting a key role through pathways such as Wnt/β-catenin (Skah et al., 2017) and Notch (Aguirre et al., 2010).

We subsequently investigated whether postnatal TH deficiency disrupts SVZ organization and, therefore, neuroglial processes. We focused on the neuron/glia balance because T_3-TRα1 represses *Sox2* to favor neuronal commitment in adult NSCs and progenitors (López-Juárez et al., 2012) and because this readout is a relevant indicator of how well NSC/progenitors might respond to brain injury

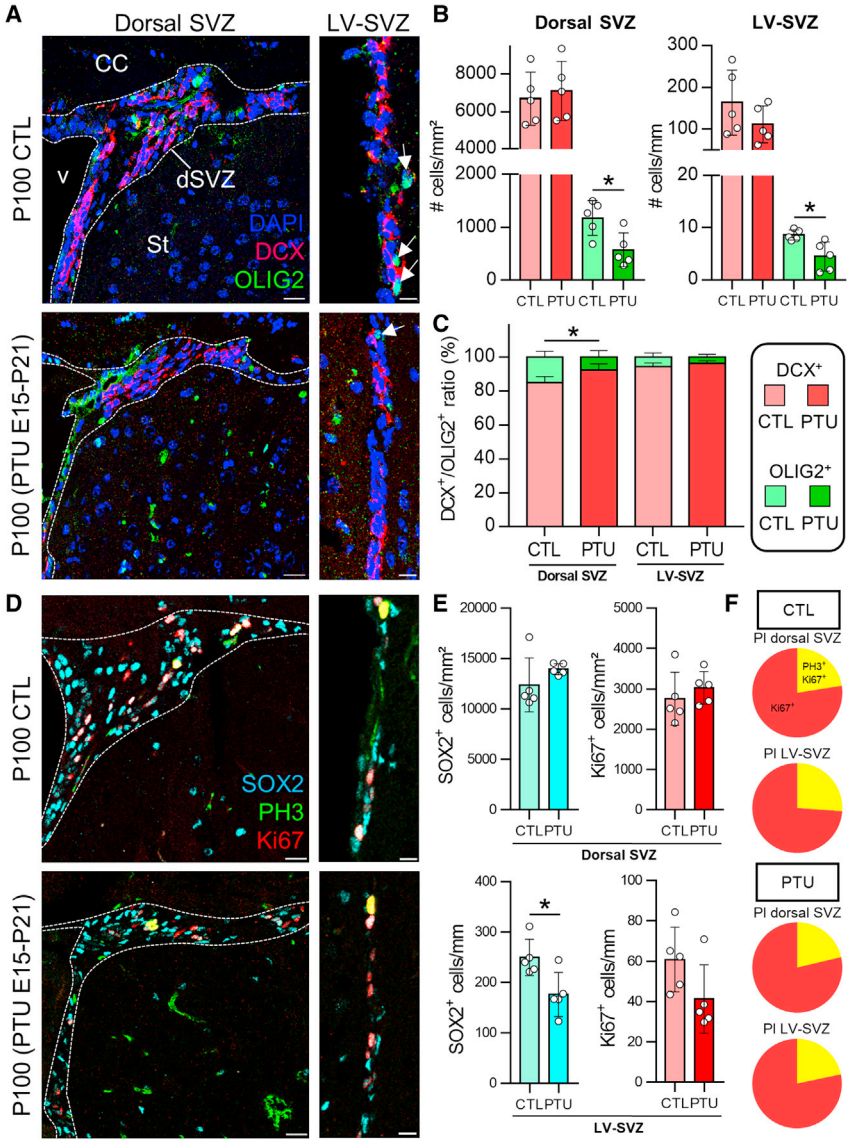

Figure 7. Reduced SVZ oligodendrogenesis in adult mice developmentally exposed to PTU

(A) Representative images of the dSVZ (left panels; scale bars, 20 μm) and LV SVZ (right panels; scale bars, 10 μm) showing DCX+ neuroblasts (red) and OLIG2+ oligodendroglia (green).

(B) Graphs (mean ± SD) showing DCX+ and OLIG2+ cell densities in the dSVZ (left) and numbers per mm in the LV SVZ (right) (n = 5/group, unpaired t test).

(C) Relative proportions of DCX+ versus OLIG2+ cells, reflecting the neuron/glia balance.

(D) Representative images of the dSVZ (left panels; scale bars, 20 μm) and lateral SVZ (right panels; scale bars, 10 μm) showing SOX2+ (light blue), PH3+ (green), and Ki67+ cells (red).

(E) Graphs (mean ± SD) showing SOX2+ and Ki67+ cell densities in the dSVZ (left) and numbers per mm in the LV SVZ (right) (n = 5, unpaired t tests, Mann-Whitney *U* test for the top left graph).

(F) Pie charts showing the proliferation index (PH3+Ki67+/Ki67+ cells). PI, proliferation index. *p < 0.05.

(Vancamp et al., 2020a). qPCR and RNAscope data showed downregulated expression of markers associated with neuroglial commitment as well as the TH target genes *Klf9* and *Dio3* as a response to low intracellular T_3. This was most profound at P15–P21, during and after the TH peak, again suggesting that SVZ NSCs respond to TH from then on. Correspondingly, before the peak at P4, we found no *in vivo* effects of PTU on neuroblast or OPC generation in the SVZ. Absence of TH regulators at P2, as shown by single-cell RNA-seq, suggested a lack of cellular machinery to respond to T_3. At P21, however, neuroblast densities in the dorsal SVZ together with *Dlx2* and *Dcx* expression decreased under PTU conditions, although OPC generation remained stable. SVZ neurogenesis was also decreased in adult mice null for *Ttr* or exposed to methimazole, although they displayed increased OPC numbers (Gothié et al., 2017; Remaud et al., 2017; Vancamp et al., 2019). Similarly, hippocampal neurogenesis was reduced in mice and rats developmentally exposed to PTU (E6–P21) or methimazole (P10–P21), respectively (Gilbert et al., 2017; Zhang et al., 2009) as well as in mice null for *Mct8* (Mayerl et al., 2020). Decreased *Olig2* expression was probably linked to reduced OPC generation in the LV SVZ at P21. Hence, TH determines neurogliogenesis in stem cell zones of the murine brain from early stages onward.

Remarkably, we found that 3-month-old mice developmentally exposed to PTU but fed a normal diet from P21 onward, had reduced OPC numbers and an altered neuron/glia ratio in the dorsal SVZ. Similarly, adult *Ttr* knockout mice that recovered from delayed brain

development (Monk et al., 2013) still had decreased SVZ neuron/glia ratios (Vancamp et al., 2019). Adult rats gestationally and perinatally treated with PTU also presented with heterotopia and aberrant cortical layering (Ausó et al., 2004; O'Shaughnessy et al., 2018). These anomalies relate to our *in vitro* results showing that NSCs cultured from P21 PTU-treated mice responded less to exogenous T_3 compared with those from control mice, indicating persistent alterations. Surprisingly, the T_3-dependent reduction in neuronal differentiation in cultured control SVZ NSCs did not match with our findings that blocked T_3 action decreased neuroblast generation *in vivo* (compare Figures 3A and 5B). In the hypothyroid adult murine SVZ, DCX+ neuroblast generation was also reduced, but a T_3 regimen enhanced neuronal differentiation in cultured SVZ NSCs from control animals (Gothié et al., 2017). This suggests that SVZ-NSCs behave differently *in vitro* when cultured during development as opposed to adult stages or because of missing factors otherwise present *in vivo*. Additionally, TH regulator expression might respond different to treatments *in vitro*. Nevertheless, the results indicate that developmental endocrine perturbation disrupts pathways underlying postnatal SVZ reorganization, misprograms NSCs permanently, and results in abnormal neuron/glia outputs later in life. In addition, although adult mice were normothyroxinemic, lower serum T_3 and higher rT_3 indicated effects on the thyroid axis and deiodinase activity as well and might aggravate inadequate TH availability control and signaling in tissues.

We also found more SOX2+ and fewer proliferating cells at P4–P21. Although TH negatively regulates *Sox2* (López-Juárez et al., 2012), decreased expression of the gene in PTU-treated newborns could be explained by cellular hypoplasia, as observed at P21 and later, too, as a consequence of reduced proliferation and perhaps increased apoptosis. In developmentally PTU-exposed adult mice, the progenitor pool in the LV SVZ was still smaller, mimicking reduced SVZ (Lemkine et al., 2005) and SGZ progenitor self-renewal following adult-onset hypothyroidism (Montero-Pedrazuela et al., 2006), in both cases rescued by TH treatment. Because SOX2 normally precedes oligodendroglial commitment (Zhang et al., 2018), it may explain lower oligodendroglia numbers in the LV SVZ. Another study found no effect on the SVZ NSC pool size in P90 rats exposed to PTU from P10–P21 (Zhang et al., 2009). Either the treatment period was too short to produce measurable effects, or TH affects NSC pool expansion primarily between E15 and P10. Previous rodent studies have already shown how the timing of goitrogen exposure determines whether a specific developmental brain malformation is detectable (O'Shaughnessy et al., 2018).

SVZ NSCs are susceptible to endocrine perturbation during crucial developmental windows, jeopardizing their future neurogliogenic properties. In the olfactory bulbs, the intertwined network of neuronal subtypes in the glomerular layer regulating olfaction was populated less densely, whereas relative proportions remained stable. As a result, adult mice failed to remember pure and distinct odors, a function dependent on adequate adult SVZ neurogenesis (Breton-Provencher et al., 2009). *Mct8/Oatp1c1* double-knockout mice displayed a similar behavioral phenotype, underlining the crucial role of TH transporters (Luongo et al., 2021). Similar impaired processes can explain why adult hypothyroid Kunming mice (Tong et al., 2007) also underperformed on short-term odor memory tests, although we cannot exclude side effects of the PTU treatment on brain development as a whole.

Reduced OPC generation could adversely modify generation of mature oligodendrocytes that promote myelin turnover (McKenzie et al., 2014) or might undermine remyelinating capacities in myelin-destructive diseases, such as multiple sclerosis. Misprogrammed SVZ NSCs could respond inadequately to brain injury, preventing repair by insufficiently replacing lost cells (Jacobs et al., 2017). Furthermore, different phenotypes in the dorsal and LV SVZs suggest that factors encoded by TH-responsive genes fine-tune neuron/glia output differently across the microdomains (Mizrak et al., 2019), some of which might be linked to gradient expression of extracellular components such as *Wnt* (Azim et al., 2014) and *Shh* (Ihrie et al., 2011).

TH is a key factor determining early NSC identity and later-life SVZ neuron/glia output in mice. Consequently, thyroid perturbation during critical windows of SVZ remodeling can reverberate long thereafter. The affected processes represent new readouts that could be used to evaluate the long-term effect of developmental EDC exposure on the brain because clear indicators are currently lacking (Ramhøj et al., 2020). Exposing mice to 100 mg/kg/day of the TH disruptor decabromodiphenyl ether from E6–P16 impaired NSC proliferation and SVZ neurogenesis and reduced calretinin interneurons in the olfactory bulbs at P16 (Xu et al., 2018). Decreased gray/white matter ratios in human offspring, reflecting altered lineage decisions in the cortex, have also been linked to altered circulating maternal TH levels (Korevaar et al., 2016). Furthermore, our data provide new insights to understand how early-life thyroid disruption can compromise later-life intellectual capacity, linking this to the alarming rise in several childhood (Gyllenberg et al., 2016) and perhaps adult neurological disorders.

EXPERIMENTAL PROCEDURES

Single-cell RNA-seq

Single-cell RNA-seq analysis was performed on publicly available datasets of *Emx1-Cre;R26-LSL-EYFP* C57BL/6J mice (Borrett et al., 2020; GEO: GSE152281). High-throughput transcriptomic profiles

were obtained using Illumina HiSeq 2500 on a 10X genomics platform. Two objects, P2-SVZ (GSM4610595) and P20-SVZ (GSM4610600), were created using the Seurat v.3.0 package in R-Studio 4.1.6 (Stuart et al., 2019). Data were log normalized and variable features selected with FindVariableFeatures() (including variance stabilizing transformation, nfeatures = 2,000). Anchors were identified with FindIntegrationAnchors() prior to integrating datasets with IntegrateData(). Principal-component analysis scaled and reduced data. A non-linear uniform manifold approximation and projection (UMAP) dimensional reduction (dim = 1,20) allowed us to cluster cell populations with FindClusters() (resolution = 0.5). FeaturePlot() visualized expression of validated markers for murine SVZ cell types (Zywitza et al., 2018) allowing us to identify and annotate cell clusters (Figure S1). The Subset() function was used to select clusters. Downstream analyses included gene expression visualization with FeaturePlot() and VlnPlot() (split.by = P2 versus P20). Co-expression plots were obtained with the Overlay() = TRUE function.

Animals

Pregnant C57BL/6J mice (E11, Janvier Labs, France) were housed at 22°C with free access to water and food. Newborns were weaned at P21. Hypothyroidism was induced by giving dams iodine-free pellets containing 0.15% PTU during a period corresponding to E15–P21 for the progeny. Mice were sacrificed via cervical dislocation. Trunk blood (3 mice/pool) was spun down (3,000 rpm, 25 min) to collect and store plasma at −20°C. For qPCR, the SVZ was dissected on ice, snap frozen, and stored at −80°C. For IHC, brains were fixed in 4% paraformaldehyde (PFA) in PBS overnight (4°C) and then in PBS 30% sucrose overnight and embedded in Tissue-Tek O.C.T. (Sakura Finetek, the Netherlands). Coronal sections (12 μm) were made on a cryostat. All experiments were approved by the CNRS ethics board and performed in strict accordance with European Directive 2010/63/EU.

Serum TH concentrations

Serum TH concentrations were measured by ultra-high performance liquid chromatography-tandem mass spectrometry (MS/MS) (Ackermans et al., 2012) with minor adaptations of sample pretreatment (de Vries et al., 2019). Briefly, 10 μL of standards in a 6% BSA matrix, serum controls, and samples were diluted with 300 μL PBS and used. Detection limits were 0.2 nmol/L for T_4 and rT_3 and 0.1 nmol/L for T_3.

Neurosphere cultures

The procedure is described in the supplemental information.

RNA extraction and qPCR

The procedure is described in the supplemental information.

RNAscope

mRNA transcripts were stained on cryosections using the RNAscope Multiplex Fluorescent Reagent Kit v.2 Assay (323100-USM; Advanced Cell Diagnostics, Hayward, CA, USA). RNAscope was performed first, excluding post-fixing tissue and protease III treatment (as in Baser et al., 2019). Slides were baked for 60 min at 60°C, dehydrated (50→70→100% ethanol), treated for 10 min with H_2O_2, and incubated in target retrieval reagent for 15 min at 98°C. The next steps were performed using the HybEZ II oven at 40°C (as in Vancamp et al., 2019). Probes (Probe-Mm-*Dio3*-O1, catalog number 562871; Probe-Mm-*Slc16a2*-C3, catalog number 545291-C3; Probe-Mm-*Thra*-C2, catalog number 519421-C2, and Probe-Mm-*Klf9*-C2, catalog number 488371-C2; ACD Technologies) were incubated for 2 h. Positive (Probe-Mm-*Ubc*) and negative (Probe-Mm-*DapB*) controls were included. Sections were then incubated with Multiplex FL v.2 Amp1 (30 min), Amp2 (30 min), and Amp3 (15 min). The fluorescent signal was developed by consecutive incubation with HRP-C1 (ACD Technologies) (15 min), Opal 570 or 690 (1/750 in TSA-Amp diluent, Akoya Biosciences) (30 min), and horseradish peroxidase (HRP) blocker (ACD Technologies) (15 min). Slides were rinsed in 1× Tris-buffered saline (TBS) + 0.2% Tween 20 prior to IHC.

Immunohistochemistry

The procedure is described in the supplemental information.

Imaging and quantification

Using a Leica TCS-SP5 confocal microscope (ImagoSeine, Université René Diderot), pictures were taken of the olfactory bulbs, *corpus callosum*, and the bilateral dorsal and LV SVZs on 3–4 sections per mouse. DAPI+ cells represented total cell numbers, allowing calculation of the proportions of marker-expressing cells. For RNAscope, each dot represented a single mRNA transcript. On 4 pictures of the dorsal SVZ per animal, transcript numbers/cell were counted in 20 randomly selected SOX2+ cells per picture. For neurospheres, 10 pictures (370 × 370 μm^2) of each replicate from each condition were taken. Counting was done with the Cell Counter plugin in FIJI.

Behavioral tests

Mice first habituated to the cotton swab and a fresh cage for 15 min. The habituation-dishabituation test comprised presentation of 5 different odors (water, lemon, orange blossom, and male and female urine). Investigation time (the relative time mice spent in close proximity [±1 cm] of the cotton wool) was measured following three consecutive presentations of 2 min with 1-min intervals. A short-term memory test measured the investigation time for 5 min of the same odor (almond) with intervals of 0, 2, 30, and 60 min.

Statistical analysis

Data were analyzed with GraphPad Prism v.9.00. Normality was tested using the Shapiro-Wilk normality test, and equality of variances was checked using the F test. Grubb's test detected possible outliers. Whenever the criteria for parametric testing were unmet, non-parametric alternatives are indicated. In the case of normal distribution, an unpaired two-tailed t test compared means of two groups; otherwise we used a Mann-Whitney *U* test. With two independent variables, a two-way ANOVA was performed, followed by a Tukey post hoc test when significant. Gene expression was evaluated with two-way ANOVA on log-transformed data, followed by a Šidák post hoc test. Matched values of behavioral tests were analyzed by two-way ANOVA followed by Bonferroni post

hoc tests. "n" refers to the number of animals (i.e., biological replicates), and technical replicate numbers are indicated in the text. Culture experiments were conducted three times (n = 3), and 10 pictures were taken per well. $p < 0.05$ was considered significant. Data are shown as scatterplots and bars depicting mean ± SD, as a heatmap for qPCR, and as violin or cluster plots for single-cell RNA-seq data. Asterisks/letters indicate statistical significance.

Data and code availability

The GEO accession number for the single-cell RNA-seq data that were analyzed in this paper is GSE152281.

SUPPLEMENTAL INFORMATION

Supplemental information can be found online at https://doi.org/10.1016/j.stemcr.2022.01.002.

AUTHOR CONTRIBUTIONS

S.R., B.A.D., and P.V. designed the study. P.V. performed the single-cell RNA-seq re-analysis. A.B. performed the TH measurements. P.V. and K.L.B. performed and analyzed the qPCR and IHC experiments. P.V. performed the RNAscope experiments. P.V., K.L.B., and A.S. performed the *in vitro* experiments. L.B. performed the behavioral studies. A.S. and S.R. assisted with dissection. P.V. collected, statistically analyzed, and interpreted the final data. P.V. made the figures and wrote the manuscript together with S.R. and B.A.D., who conceptualized and supervised the experiments. All authors read and approved the final manuscript.

CONFLICTS OF INTERESTS

The authors declare no competing interests.

ACKNOWLEDGMENTS

We thank the ImagoSeine platform of the Institut Jacques Monod (Université René Diderot). We also thank Fabien Uridat and Stéphane Sosinsky for excellent animal care. P.V. was supported by the European Thyroid Association (basic science grant) and the Fondation pour la Recherche Médicale (SPF201909009111). This work was additionally supported by the Centre National de la Recherche Scientifique and the Muséum National d'Histoire Naturelle, NeurATRIS (IONESCO grant), and the EU H2020 contract ATHENA (666869).

Received: June 11, 2021
Revised: January 4, 2022
Accepted: January 4, 2022
Published: February 3, 2022

REFERENCES

Ackermans, M.T., Kettelarij-Haas, Y., Boelen, A., and Endert, E. (2012). Determination of thyroid hormones and their metabolites in tissue using SPE UPLC-tandem MS. Biomed. Chromatogr. *26*, 485–490.

Aguirre, A., Rubio, M.E., and Gallo, V. (2010). Notch and EGFR pathway interaction regulates neural stem cell number and self-renewal. Nature *467*, 323–327.

Amano, I., Takatsuru, Y., Khairinisa, M.A., Kokubo, M., Haijima, A., and Koibuchi, N. (2018). Effects of mild perinatal hypothyroidism on cognitive function of adult male offspring. Endocrinology *159*, 1910–1921.

Ausó, E., Lavado-Autric, R., Cuevas, E., del Rey, F.E., Morreale de Escobar, G., and Berbel, P. (2004). A moderate and transient deficiency of maternal thyroid function at the beginning of fetal neocorticogenesis alters neuronal migration. Endocrinology *145*, 4037–4047.

Azim, K., Fischer, B., Hurtado-Chong, A., Draganova, K., Cantù, C., Zemke, M., Sommer, L., Butt, A., and Raineteau, O. (2014). Persistent wnt/β-catenin signaling determines dorsalization of the postnatal subventricular zone and neural stem cell specification into oligodendrocytes and glutamatergic neurons. Stem Cells *32*, 1301–1312.

Bárez-López, S., and Guadaño-Ferraz, A. (2017). Thyroid hormone availability and action during brain development in rodents. Front. Cell. Neurosci. *11*, 240.

Baser, A., Skabkin, M., Kleber, S., Dang, Y., Gülcüler Balta, G.S., Kalamakis, G., Göpferich, M., Ibañez, D.C., Schefzik, R., Lopez, A.S., et al. (2019). Onset of differentiation is post-transcriptionally controlled in adult neural stem cells. Nature *566*, 100–104.

Bianco, A.C., Dumitrescu, A., Gereben, B., Ribeiro, M.O., Fonseca, T.L., Fernandes, G.W., and Bocco, B.M.L.C. (2019). Paradigms of dynamic control of thyroid hormone signaling. Endocr. Rev. *40*, 1000–1047.

Boas, M., Feldt-Rasmussen, U., and Main, K.M. (2012). Thyroid effects of endocrine disrupting chemicals. Mol. Cell. Endocrinol. *355*, 240–248.

Borrett, M.J., Innes, B.T., Jeong, D., Tahmasian, N., Storer, M.A., Bader, G.D., Kaplan, D.R., and Miller, F.D. (2020). Single-cell profiling shows murine forebrain neural stem cells reacquire a developmental state when activated for adult neurogenesis. Cell Rep. *32*, 108022.

Breton-Provencher, V., Lemasson, M., Peralta, M.R., and Saghatelyan, A. (2009). Interneurons produced in adulthood are required for the normal functioning of the olfactory bulb network and for the execution of selected olfactory behaviors. J. Neurosci. *29*, 15245–15257.

Dugas, J.C., Ibrahim, A., and Barres, B.A. (2012). The T3-induced gene KLF9 regulates oligodendrocyte differentiation and myelin regeneration. Mol. Cell. Neurosci. *50*, 45–57.

Fuentealba, L.C., Rompani, S.B., Parraguez, J.I., Obernier, K., Romero, R., Cepko, C.L., and Alvarez-Buylla, A. (2015). Embryonic origin of postnatal neural stem cells. Cell *161*, 1644–1655.

Gilbert, M.E., Goodman, J.H., Gomez, J., Johnstone, A.F.M., and Ramos, R.L. (2017). Adult hippocampal neurogenesis is impaired by transient and moderate developmental thyroid hormone disruption. Neurotoxicology *59*, 9–21.

Gothié, J., Vancamp, P., Demeneix, B., and Remaud, S. (2020). Thyroid hormone regulation of neural stem cell fate: from development to ageing. Acta Physiol. *228*, e13316.

Gothié, J.D., Sébillot, A., Luongo, C., Legendre, M., Nguyen Van, C., Le Blay, K., Perret-Jeanneret, M., Remaud, S., and Demeneix, B.A. (2017). Adult neural stem cell fate is determined by thyroid hormone activation of mitochondrial metabolism. Mol. Metab. *6*, 1551–1561.

Gyllenberg, D., Sourander, A., Surcel, H.-M., Hinkka-Yli-Salomäki, S., McKeague, I.W., and Brown, A.S. (2016). Hypothyroxinemia during gestation and offspring schizophrenia in a national birth cohort. Biol. Psychiatry *79*, 962–970.

Hadj-Sahraoui, N., Seugnet, I., Ghorbel, M.T., and Demeneix, B. (2000). Hypothyroidism prolongs mitotic activity in the post-natal mouse brain. Neurosci. Lett. *280*, 79–82.

Hernandez, A., Morte, B., Belinchón, M.M., Ceballos, A., and Bernal, J. (2012). Critical role of types 2 and 3 deiodinases in the negative regulation of gene expression by T3 in the mouse cerebral cortex. Endocrinology *153*, 2919–2928.

Ihrie, R.A., Shah, J.K., Harwell, C.C., Levine, J.H., Guinto, C.D., Lezameta, M., Kriegstein, A.R., and Alvarez-Buylla, A. (2011). Persistent sonic hedgehog signaling in adult brain determines neural stem cell positional identity. Neuron *71*, 250–262.

Jacobs, M.N., Marczylo, E.L., Guerrero-Bosagna, C., and Rüegg, J. (2017). Marked for life: epigenetic effects of endocrine disrupting chemicals. Annu. Rev. Environ. Resour. *42*, 105–160.

Korevaar, T.I.M.M., Muetzel, R., Medici, M., Chaker, L., Jaddoe, V.W.V.V., de Rijke, Y.B., Steegers, E.A.P.P., Visser, T.J., White, T., Tiemeier, H., et al. (2016). Association of maternal thyroid function during early pregnancy with offspring IQ and brain morphology in childhood: a population-based prospective cohort study. Lancet Diabetes Endocrinol. *4*, 35–43.

Lemkine, G.F., Raji, A., Alfama, G., Turque, N., Hassani, Z., Alegria-Prévot, O., Samarut, J., Levi, G., and Demeneix, B.A. (2005). Adult neural stem cell cycling in vivo requires thyroid hormone and its alpha receptor. FASEB J. *19*, 1–17.

Lim, D.A., and Alvarez-Buylla, A. (2016). The adult ventricular–subventricular zone (V-SVZ) and olfactory bulb (OB) neurogenesis. Cold Spring Harb. Perspect. Biol. *8*, a018820.

López-Espíndola, D., García-Aldea, Á., Gómez de la Riva, I., Rodríguez-García, A.M., Salvatore, D., Visser, T.J., Bernal, J., and Guadaño-Ferraz, A. (2019). Thyroid hormone availability in the human fetal brain: novel entry pathways and role of radial glia. Brain Struct. Funct. *224*, 2103–2119.

López-Juárez, A., Remaud, S., Hassani, Z., Jolivet, P., Pierre Simons, J., Sontag, T., Yoshikawa, K., Price, J., Morvan-Dubois, G., and Demeneix, B.A. (2012). Thyroid hormone signaling acts as a neurogenic switch by repressing Sox2 in the adult neural stem cell niche. Cell Stem Cell. *10*, 531–543.

Luongo, C., Butruille, L., Sébillot, A., Le Blay, K., Schwaninger, M., Heuer, H., Demeneix, B.A., and Remaud, S. (2021). Absence of both thyroid hormone transporters MCT8 and OATP1C1 impairs neural stem cell fate in the adult mouse subventricular zone. Stem Cell Rep. *16*, 337–353.

Mayerl, S., Heuer, H., and Ffrench-Constant, C. (2020). Hippocampal neurogenesis requires cell-autonomous thyroid hormone signaling. Stem Cell Rep. *14*, 845–860.

McKenzie, I.A., Ohayon, D., Li, H., Paes de Faria, J., Emery, B., Tohyama, K., and Richardson, W.D. (2014). Motor skill learning requires active central myelination. Science *346*, 318–322.

Menn, B., Garcia-Verdugo, J.M., Yaschine, C., Gonzalez-Perez, O., Rowitch, D., and Alvarez-Buylla, A. (2006). Origin of oligodendrocytes in the subventricular zone of the adult brain. J. Neurosci. *26*, 7907–7918.

Merkle, F.T., Tramontin, A.D., Garcia-Verdugo, J.M., and Alvarez-Buylla, A. (2004). Radial glia give rise to adult neural stem cells in the subventricular zone. Proc. Natl. Acad. Sci. U S A *101*, 17528–17532.

Mizrak, D., Levitin, H.M., Delgado, A.C., Crotet, V., Yuan, J., Chaker, Z., Silva-Vargas, V., Sims, P.A., and Doetsch, F. (2019). Single-cell analysis of regional differences in adult V-SVZ neural stem cell lineages. Cell Rep. *26*, 394–406.e5.

Monk, J.A., Sims, N.A., Dziegielewska, K.M., Weiss, R.E., Ramsay, R.G., and Richardson, S.J. (2013). Delayed development of specific thyroid hormone-regulated events in transthyretin null mice. Am. J. Physiol. Metab. *304*, E23–E31.

Montero-Pedrazuela, A., Venero, C., Lavado-Autric, R., Fernández-Lamo, I., García-Verdugo, J.M., Bernal, J., and Guadaño-Ferraz, A. (2006). Modulation of adult hippocampal neurogenesis by thyroid hormones: implications in depressive-like behavior. Mol. Psychiatry. *11*, 361–371.

Moog, N.K., Entringer, S., Heim, C., Wadhwa, P.D., Kathmann, N., and Buss, C. (2017). Influence of maternal thyroid hormones during gestation on fetal brain development. Neuroscience *342*, 68–100.

Mughal, B.B., Fini, J.-B., and Demeneix, B.A. (2018). Thyroid-disrupting chemicals and brain development: an update. Endocr. Connect. *7*, R160–R186.

O'Shaughnessy, K.L., Kosian, P.A., Ford, J.L., Oshiro, W.M., Degitz, S.J., and Gilbert, M.E. (2018). Developmental thyroid hormone insufficiency induces a cortical brain malformation and learning impairments: a cross-fostering study. Toxicol. Sci. *163*, 101–115.

Ramhøj, L., Hass, U., Gilbert, M.E., Wood, C., Svingen, T., Usai, D., Vinggaard, A.M., Mandrup, K., and Axelstad, M. (2020). Evaluating thyroid hormone disruption: investigations of long-term neurodevelopmental effects in rats after perinatal exposure to perfluorohexane sulfonate (PFHxS). Sci. Rep. *10*, 2672.

Remaud, S., Ortiz, F.C., Perret-Jeanneret, M., Aigrot, M.-S., Gothié, J.-D., Fekete, C., Kvárta-Papp, Z., Gereben, B., Langui, D., Lubetzki, C., et al. (2017). Transient hypothyroidism favors oligodendrocyte generation providing functional remyelination in the adult mouse brain. Elife *6*, e29996.

Roberts, L.M., Woodford, K., Zhou, M., Black, D.S., Haggerty, J.E., Tate, E.H., Grindstaff, K.K., Mengesha, W., Raman, C., and Zerangue, N. (2008). Expression of the thyroid hormone transporters monocarboxylate transporter-8 (SLC16A2) and organic ion transporter-14 (SLCO1C1) at the blood-brain barrier. Endocrinology *149*, 6251–6261.

Rushing, G., and Ihrie, R.A. (2016). Neural stem cell heterogeneity through time and space in the ventricular-subventricular zone. Front. Biol. *11*, 261–284.

Skah, S., Uchuya-Castillo, J., Sirakov, M., and Plateroti, M. (2017). The thyroid hormone nuclear receptors and the Wnt/β-catenin pathway: an intriguing liaison. Dev. Biol. *422*, 71–82.

Stuart, T., Butler, A., Hoffman, P., Hafemeister, C., Papalexi, E., Mauck, W.M., Hao, Y., Stoeckius, M., Smibert, P., and Satija, R. (2019). Comprehensive integration of single-cell data. Cell *177*, 1888–1902.e21.

Tong, H., Chen, G.-H., Liu, R.-Y., and Zhou, J.-N. (2007). Age-related learning and memory impairments in adult-onset hypothyroidism in Kunming mice. Physiol. Behav. *91*, 290–298.

Vancamp, P., Gothié, J.-D., Luongo, C., Sébillot, A., Le Blay, K., Butruille, L., Pagnin, M., Richardson, S.J., Demeneix, B.A., and Remaud, S. (2019). Gender-specific effects of transthyretin on neural stem cell fate in the subventricular zone of the adult mouse. Sci. Rep. *9*, 19689.

Vancamp, P., Butruille, L., Demeneix, B.A., and Remaud, S. (2020a). Thyroid hormone and neural stem cells: repair potential following brain and spinal cord injury. Front. Neurosci. *14*, 875.

Vancamp, P., Demeneix, B.A., and Remaud, S. (2020b). Monocarboxylate transporter 8 deficiency: delayed or permanent hypomyelination? Front. Endocrinol. *11*, 283.

de Vries, E.M., Surovtseva, O., Vos, W.G., Kunst, R.F., van Beeren, M., Kwakkel, J., Chassande, O., Ackermans, M.T., Fliers, E., and Boelen, A. (2019). Downregulation of type 3 deiodinase in the hypothalamus during inflammation. Thyroid *29*, 1336–1343.

Williams, G.R. (2008). Neurodevelopmental and neurophysiological actions of thyroid hormone. J. Neuroendocrinol. *20*, 784–794.

Wilpert, N.-M., Krueger, M., Opitz, R., Sebinger, D., Paisdzior, S., Mages, B., Schulz, A., Spranger, J., Wirth, E.K., Stachelscheid, H., et al. (2020). Spatiotemporal changes of cerebral monocarboxylate transporter 8 expression. Thyroid *30*, 1366–1383.

Xu, M., Huang, Y., Li, K., Cheng, X., Li, G., Liu, M., Nie, Y., Geng, S., and Zhao, S. (2018). Developmental exposure of decabromodiphenyl ether impairs subventricular zone neurogenesis and morphology of granule cells in mouse olfactory bulb. Arch. Toxicol. *92*, 529–539.

Zhang, L., Blomgren, K., Kuhn, H.G., and Cooper-Kuhn, C.M. (2009). Effects of postnatal thyroid hormone deficiency on neurogenesis in the juvenile and adult rat. Neurobiol. Dis. *34*, 366–374.

Zhang, S., Zhu, X., Gui, X., Croteau, C., Song, L., Xu, J., Wang, A., Bannerman, P., and Guo, F. (2018). Sox2 is essential for oligodendroglial proliferation and differentiation during postnatal brain myelination and CNS remyelination. J. Neurosci. *38*, 1802–1820.

Zywitza, V., Misios, A., Bunatyan, L., Willnow, T.E., and Rajewsky, N. (2018). Single-cell transcriptomics characterizes cell types in the subventricular zone and uncovers molecular defects impairing adult neurogenesis. Cell Rep. *25*, 2457–2469.e8.